Formation and growth of palladium nanoparticles inside porous poly(4-vinyl-pyridine) monitored by operando techniques: The role of different reducing agents

UNIVERSITÀ DEGLI STUDI DI TORINO

Formation and growth of palladium nanoparticles inside porous poly(4-vinyl-pyridine) monitored by operando techniques: The role of different reducing agents

Andrea Lazzarini[a,**], Elena Groppo[a], Giovanni Agostini[b], Elisa Borfecchia[a], Francesco Giannici[c], Giuseppe Portale[d], Alessandro Longo[e,f], Riccardo Pellegrini[g], Carlo Lamberti[h,i,*]

[a]Dept. of Chemistry, NIS and INSTM Reference Centers, University of Torino, Via Quarello 15, I-10135 Torino, Italy.
[b]European Synchrotron Radiation Facility (ESRF), 71 avenue des Martyrs, 38000 Grenoble, France.
[c]Dipartimento di Fisica e Chimica, Università di Palermo, viale delle Scienze, I-90128 Palermo, Italy.
[d]Univ. Groningen, Zernike Inst. Adv. Mat. Macromol. Chem. & New Polymer Mat., Nijenborgh 4, NL-9747 AG Groningen, The Netherlands.
[e]Netherlands Organization for Scientific Research at ESRF, BP 220, F-38043 Grenoble Cedex 9, France.
[f]Istituto per lo Studio dei Materiali Nanostrutturati, Sezione di Palermo, Consiglio Nazionale delle Ricerche, Via La Malfa, 153, I-90146 Palermo, Italy.
[g]Chimet SpA—Catalyst Division, Via di Pescaiola 74, Viciomaggio Arezzo, I-52041, Italy.
[h]IRC "Smart Materials", Southern Federal University, Zorge street 5, 344090, Rostov-on-Don, Russia.
[i]Dept. of Chemistry, CrisDi Centre for Crystallography, University of Torino, Via Giuria 7, I-10125 Torino, Italy.
*Corresponding author at: IRC "Smart Materials", Southern Federal University, Zorge street 5, 344090, Rostov-on-Don, Russia. Email: carlo.lamberti@unito.it
**Corresponding author at: Dept. of Chemistry, NIS and INSTM Reference Centers, University of Torino, Via Quarello 15, I-10135 Torino, Italy. Email: andrea.lazzarini@unito.it

Abstract

In this work we followed the formation of palladium nanoparticles, starting from palladium (II) acetate precursor, inside a poly(4-vinylpyridine-co-divinylbenzene) polymer in presence of different reducing agents. The formation and growth of palladium nanoparticles in presence of H2was followed as a function of temperature by simultaneous XANES-SAXS techniques, coupled with DRIFT spectroscopy in operando conditions. It was found that the pyridyl functional groups in the polymer plays a fundamental role in the stabilization of the palladium (II) acetate precursor, as well as in the stabilization of the palladium nanoparticles. The effect of a thermal treatment in alcohol (ethanol and 2-propanol) was preliminarily investigated by means of DRIFT spectroscopy in operando conditions. We found that alcohols act as reducing agents for Pd(OAc)2. The obtained palladium nanoparticles were preliminarily characterized by means of IR spectroscopy using CO as probe molecule.

1. Introduction

Metal nanoparticles supported on high-surface-area supports are fundamental materials for catalytic applications exhibiting enhanced performances compared to unsupported metal nanoparticles and homogeneous catalysts. In fact, support prevents particles growth and aggregation and allows an easier separation and recovery of the spent catalyst from reaction mixture. Considering the whole branch of heterogeneous catalysts com-posed of metal nanoparticles, those based on palladium are widely employed in several applications, in combination with various sup-ports having organic (such as carbons) or inorganic (Al2O3, SiO2, and others) nature [1–3]. In particular, palladium nanoparticles supported on porous polymers are a promising class of catalysts showing physical chemical properties different from the most com-mon carbon-based or oxide-based catalysts and attractive catalytic performances [4–13]. For example, polymer-supported palladium-based catalysts have shown remarkable performance in coupling and hydrogenation reactions [14]. The polymer may act simultaneously as support and stabilizer, thanks to the dual effect of porosity (steric stabilization) and polar functional groups (electrostatic stabilization) [15–17]. In polymers without specific functional groups, such as polystyrene-based polymers, stabilization occurs only via electronic interaction between the π electrons of the benzene rings of the polymer and the empty orbitals of metal atoms [11,18,19]. For polymers having specific functional groups, instead, an additional stabilization mechanism, involving a σ-type coordination between hetero-donor atoms of the functional groups and the sur-face of metal nanoparticles, may take place. This is an effect similar to what occurs in solution in the presence of classical stabilizers, such as carboxylic acids, thiols, or amines [20]. Highly cross-linked porous polymers with functional groups combine the two stabilization mechanisms, steric and electrostatic (dipole-charge or dipole–dipole interactions). Recently, we undertook a thorough investigation of palladium-based catalysts supported on highly cross-linked porous polymers with and without functional groups [21–23]. In recent papers [21–23], we proved that the reduction of palladium precursor(palladium(II) acetate), in the presence of H2or CO, can be monitored by applying simultaneously Small-Angle X-ray Scattering (SAXS) [24–26] and X-ray Absorption Near Edge Structure (XANES) [27–29] techniques and Diffuse Reflectance Infrared Fourier Transform (DRIFT) spectroscopy [30–32] in operando conditions. We found that in presence of functional groups, such as the pyridyl group in poly(4-vinylpyridine-co-divinylbenzene), palladium (II) acetate is stabilized through the coordination of Pd^{2+} cations, with the consequent rupture of the trimeric structure characteristic for solid palladium (II) acetate, and the restructuring of the acetate ligands in a monodentate coordination. In addition, extremely small (<2 nm) and very homogeneous palladium nanoparticles are formed upon H_2 reduction [21], compared to those obtained in polymers without functional groups, such as poly(ethylstyrene-co-divinylbenzene). Herein we extend our previous study to investigate the behavior of palladium (II) acetate inside the same poly(4-vinylpyridine-co-divinylbenzene) matrix, but in presence of alcohols as reducing agents. Indeed, palladium-catalyzed reactions (e.g. hydrogenation, Suzuki-Miyaura Cross-Coupling reaction, and others) [33] are often conducted in slurry conditions, using alcohols as solvents, because alcohols combine good solvation properties for organic compounds with a low price. Hence, understanding the role of alcohols in palladium-catalyzed reactions is of prime interest in the optimization of the reaction variables. In other cases, alcohols are used as reactants. For example, alcohol hydrogenation, oxidation and cross-coupling reactions are also catalyzed by palladium-based catalysts, either homogeneous or heterogeneous [34–41]. In this respect, the homogeneous $Pd(OAc)_2$/pyridine system is by far one of the most efficient and selective catalyst for oxidation of alcohols to aldehydes. The reaction mechanism has been proposed by Stahl and coworkers [38–40] as an oxidase-style mechanism in which palladium(II)-mediated substrate oxidation (Stage I in Scheme 1) and aerobic oxidation of the catalyst (Stage II in Scheme 1) occur in two independent, sequential stages. Formally, in Stage I Pd(II) species transform into Pd^0 ones, while in the Stage II oxidation by oxygen restores the Pd(II) original complex. These steps occur with the contemporary elimination (Stage I) or addition (Stage II) of acetic ligands. The main cause of deactivation for the homogeneous $Pd(OAc)_2$/pyridine catalyst is

the formation of metal nanoparticles, which occurs when Stage II is inhibited, that is in absence of oxygen. In our prospect, the palladium (II) acetate inside the porous poly(4-vinylpyridine-co-divinylbenzene) matrix may show catalytic behavior similar to the $Pd(OAc)_2$/pyridine system, provided that the reaction conditions (reagents mixture, temperature, etc.) are properly set. To this aim it is important to understand the effect of alcohols on P4VP/$Pd(OAc)_2$, in absence and in presence of oxygen, as a function of the reaction temperature. The present paper deals with the first step (understanding the role of alcohols in absence of oxygen), while the second step will be the subject of a successive work. Since alcohols are mild reducing agents, the redox behavior of palladium (II) acetate inside poly(4-vinylpyridine-co-divinylbenzene) in presence of H_2 as a function of temperature is discussed first. In particular, we summarize our recent results obtained by applying: (i) simultaneous XANES-SAXS techniques, which give direct information on the oxidation state and electronic density of the palladium phase; (ii) operando DRIFT spectroscopy, which gives information on the acetate ligands; and (iii) IR spectroscopy of adsorbed CO, which provides information on the surface properties of palladium nanoparticles. In the second part of the paper we present DRIFT data in operando on the effects of different alcohols (ethanol and 2-propanol) on the same system as a function of temperature.

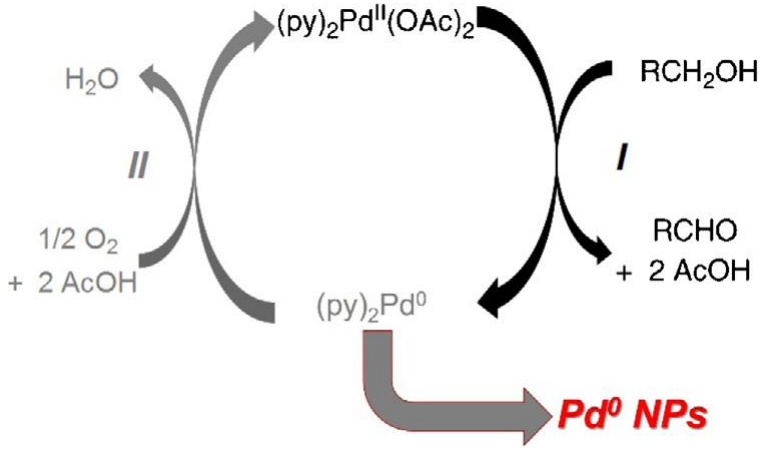

Scheme 1. Catalytic cycle for alcohol aerobic oxidation catalyzed by homogeneous $Pd(OAc)_2$/Pyridine catalyst as proposed by Stahl et al. [38–40]. Stage I (black arrows) involves alcohol oxidation into aldehyde/ketone by eliminating acetate ions as acetic acid; Stage II (grey arrows) involves the active species regeneration, by converting acetic acid and O_2 into acetate ions and water. The absence or the loss of efficiency of Stage II, results in the formation of precipitated Pd^0 nanoparticles, causing the deactivation of the catalyst in the homogeneous phase.

2. Sample and Methods

2.1. Investigated catalyst

The starting catalyst was obtained by impregnating a commercial poly(4-vinylpyridine-co-divinylbenzene) polymer (P4VP hereafter), commercialized by Sigma Aldrich, with a solution of palladium (II) acetate ($Pd(OAc)_2$ hereafter) in acetonitrile, having a final palladium loading of 5 wt.%. The polymeric support has a specific surface area of about 50 $m^2 \cdot g^{-1}$, which is relatively poor compared to other supports [21]. However the presence of the pyridyl group plays a fundamental role in the dispersion and in the stabilization of the palladium precursor. After impregnation, the sample was dried at room temperature. Finally, the sample was gently grinded in a mortar in order to obtain a powder.

2.2. Experimental methods

FT–IR spectra were collected in diffuse reflectance mode (DRIFT) on a Nicolet 6700 instrument, equipped with a MCT detector, using a Thermo Fisher Environmental Chamber to record data under reaction conditions. FT-IR spectra were recorded at regular temperature intervals during the whole reaction at a spectral resolution

of 4 cm^{-1}, averaging 64 spectra. Thermal treatments in presence of H_2 or alcohols were performed following a temperature ramp of 2 °C·min^{-1}, from 25 °C up to 200 °C. The cell was connected to a gas-flow system (under atmospheric pressure), equipped with Brooks Instrument Delta Smart Mass Flow Controllers (MFC), controlled via Read Out & Control Electronics 0154 by Brooks Instrument. The MFCs were calibrated for each gas used using Agilent Optiflow 570instrument. A total flow of 25 ml·min^{-1} was used. Reduction was performed either in H_2 (5% H_2 in N_2), or in presence of alcohols (ethanol and 2-propanol). In the latter cases, vapors of alcohols were dosed from the liquids at room temperature, exploiting a 25 ml·min^{-1} N_2 stream. After the reduction step, the sample was cooled at room temperature in inert atmosphere. Successively, 50% CO in N_2 (total flow = 25 ml·min^{-1}) was dosed, in order to investigate the eventual formation of the nanoparticles and their surface properties. Simultaneous XANES-SAXS measurements were performed on the BM26A beamline at the ESRF facility (Grenoble, France), by using the experimental set-up discussed elsewhere [42,43]. The samples in powder form were placed in a 2 mm glass capillary connected to a gas flow system, and heated with a heat gun. Thermal treatments and gas dosing were the same applied during the DRIFT measurements. Fluorescence XANES spectra at the Pd K edge (24.35 keV) were collected with a 9-element Ge detector. A double crystal Si(111) monochromator was used; the energy delivered was calibrated measuring the XANES spectrum of a palladium foil in transmission mode. The spectra were normalized and treated with the Athena software [44]. The SAXS patterns were collected by using a 2D Mar CCD detector. The sample-to-detector distance was calibrated according to the peak position of a standard Ag behenate powder sample. The energy change during XANES measurements (about 120 eV: $\Delta E/E = \Delta\lambda/\lambda < 5 \times 10^{-3}$) was irrelevant to SAXS collected with a photon energy so high that the incident beam wavelength can be treated as constant, λ = 0.509(1) Å. The resulting q-range was 0.5–7 nm^{-1} (with the module of the scattering vector $q = 4\pi \sin\theta/\lambda$, in which θ is half of the scattering angle), allowing to investigate the 12.5–0.7 nm d-spacing interval ($d = 2\pi/q$). We decided to collect a single XANES/SAXS spectrum/pattern in 300 s, corresponding to a temperature increase of Δt = 10 °C during the reduction treatment. As the readout and erasing time of the SAXS detector was of 180 s, each XANES spectrum was collected with an integration statistics of 120 s; in such a way we obtained a 1:1 correspondence between XANES spectra and SAXS patterns. According with this acquisition strategy, 16 combined XANES/SAXS spectra/patterns were collected along the thermal activation in H_2 flow from RT to 200 °C. Four additional data XANES/SAXS collections were successively collected in isotherm condition at 200 °C. The SAXS data have been analysed by fitting the experimental patterns with the function described by Eq. (1):

$$I(q) = A + \frac{B}{q^4} + C \int D(r) j(qR)^2 r^6 dr \qquad (1)$$

in which the term $A + B/q^4$ describes the Porod function [45], simulating the polymer contribution; $D(r)$ corresponds to the Weibull function, accounting for the particle size distribution, defined as $D(r) = (r/R)^{-1} exp(-r/R)^b$, in which R is the average radius of the particles; and $j(qR)$ is the first order Bessel function, accounting for spherical shape of the metal clusters.

3. Results and Discussion

3.1. H_2 activation

3.1.1. Simultaneous SAXS-XANES

It has been demonstrated that SAXS and XANES techniques applied simultaneously under reduction conditions provide information on the evolution of the palladium oxidation state, the size of the formed palladium nanoparticles or aggregates and the quantity of palladium contributing to the total scattering as a function of both time and temperature [22,23,46–49]. Fig. 1 shows the evolution of the normalized XANES spectra (part a) and SAXS patterns (reported in a log–log plot, part b) at the Pd K-edge, collected simultaneously during thermal treatment of P4VP/$Pd(OAc)_2$ in gaseous H_2 (5% H_2 in He) from room temperature (purple) to 200 °C

(red). During the reaction, the XANES spectra (Fig. 1a) change gradually, as a result of the progressive reduction of the Pd^{2+} precursor and the formation of palladium metal nanoparticles. In particular, the edge shifts to lower energy, the white-line is flattened and a weak band grows at 24393 eV, ascribable to the first EXAFS oscillation of palladium atoms arranged in an fcc structure [21–23]. The evolution of the spectra can be better appreciated by observing them in first derivative (inset in Fig. 1a). The energy position of feature 1 (ΔE_1) and the intensity of feature 2 (ΔI_2) in the first derivative spectra are shown as a function of temperature in Fig. 2a. ΔE_1 changes according to the edge position and gives information on the oxidation state of palladium. It is evident that almost no reduction occurs up to 110 °C. The growth of ΔI_2 roughly correlates with the dimension of the formed nanoparticles. Feature 2 grows as soon as feature 1 starts to change. The final intensity of feature 2 (0.02 eV^{-1}) is much smaller with respect to that observed for palladium metal foil (0.04 eV^{-1}) [21], as expected for nanoparticles, due to the relevant fraction of low-coordination surface sites compared to the total amount of metal sites [50–52]. Complementary information regarding the palladium particle size can be obtained by the analysis of SAXS data.

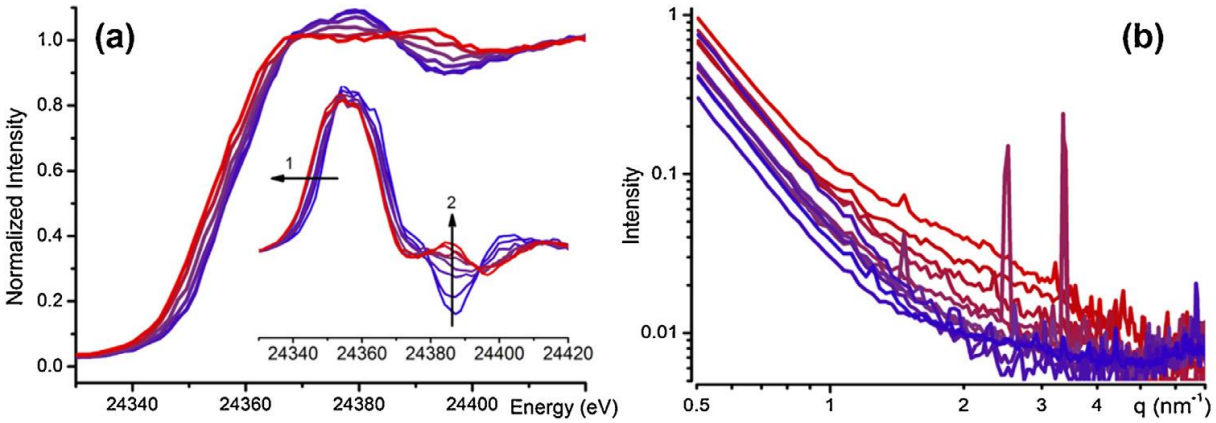

Fig. 1. Selection of spectra showing the evolution of the normalized Pd K-edge XANES spectra (part a) and SAXS patterns (in log–log scale, part b) collected simultaneously during reduction of P4VP/$Pd(OAc)_2$ in H_2 from room temperature (purple) to 200 °C (red) with a heating rate of 2 °C·min^{-1}; inset of part a shows the derivative of normalized XANES spectra. (For interpretation of the references to colour in this figure legend, the reader is referred to the web version of this article).

Fig. 1b shows the evolution of I(q) vs the modulus of scattering vector (q) in logarithmic scale for P4VP/$Pd(OAc)_2$ as a function of temperature during the heating ramp in gaseous H_2. The patterns begin to change above 110 °C, in perfect agreement with the XANES data previously discussed. The SAXS data reported in Fig. 1b have been analysed by fitting the experimental patterns with the function described in Section 2.2. by Eq. (1). Fig. 2b shows the evolution of the mean particle diameter (<dSAXS> = 2R) obtained from such analysis. Below 110 °C the particle diameter remains almost constant around <dSAXS> = 0.70 ± 0.05 nm. When reduction of palladium (II) acetate begins to occur, the average particle size increases up to a value around 1.50 ± 0.05 nm, in good agreement with previous data reported for P4VP/$Pd(OAc)_2$ sample reduced in H_2 in static conditions [21]. Once reached 200 °C the system was kept in isothermal condition for 20 min without observing any significant change neither in the XANES spectra nor in the SAXS patterns. This additional information confirms that the metal nanoparticle formation is complete at the end of the activation ramp in H_2 at 200 °C. A final relevant aspect of the operando XANES/SAXS study needs to be clarified. While the XANES technique is element-selective, reporting information related to Pd atoms only, SAXS is not. Actually, due to the dilution of the Pd species, the largest contribution to the SAXS signal comes from the P4VP support. To validate the solidity of our SAXS data analysis (Fig. 2b) we must consequently demonstrate that possible evolution of the Pd4VP structure (e.g. changes in the pore distributions) along the thermal treatment in H_2 flow up to 200 °C has a negligible effect on the SAXS profile of the polymer itself. To prove this thesis, the same SAXS experiment reported in Fig. 1b for the P4VP/$Pd(OAc)_2$ system has been repeated on the bare P4VP

support and reported in Fig. 3. The evolution of the SAXS patterns of P4VP along the thermal activation in H_2 from room temperature (bold red pattern) to 200 °C (bold blue pattern) is minimal, and mainly limited in the 0.7–1.2 nm^{-1} range, while the Pd nanoparticle formation affects the SAXS profile mainly in the 1.5–4.2 nm^{-1} range and in a much larger extent (Fig. 1b). Consequently, we can safely conclude that the changes observed in the SAXS patterns of P4VP/$Pd(OAc)_2$ are almost entirely due to changes in the supported Pd phase, and that the quantitative SAXS analysis reported in Fig. 2b is not biased by any significant systematic error due to changes in the scattering from the polymer support.

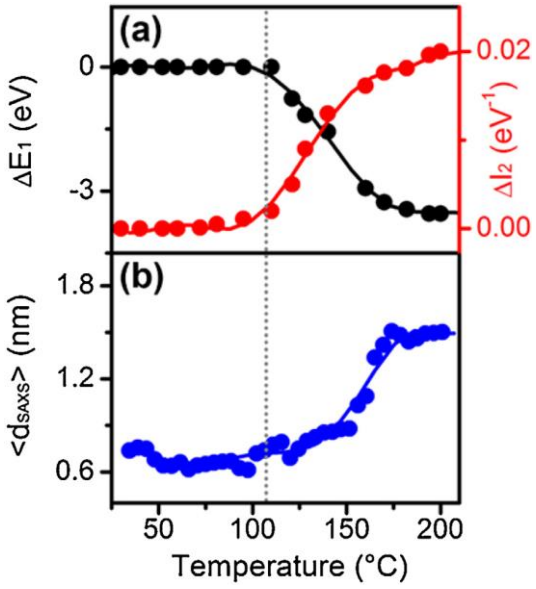

Fig. 2. Analysis of the XANES and XAS data collected during the reduction of P4VP/$Pd(OAc)_2$ in H_2 as a function of temperature. Part (a): evolution of feature 1 (shift in energy-black curve) and feature 2 (change in intensity-red curve) in the derivative XANES spectra (see inset in Fig. 1a). Part (b): average palladium particle size as obtained from analysis of the SAXS data. (For interpretation of the references to colour in this figure legend, the reader is referred to the web version of this article).

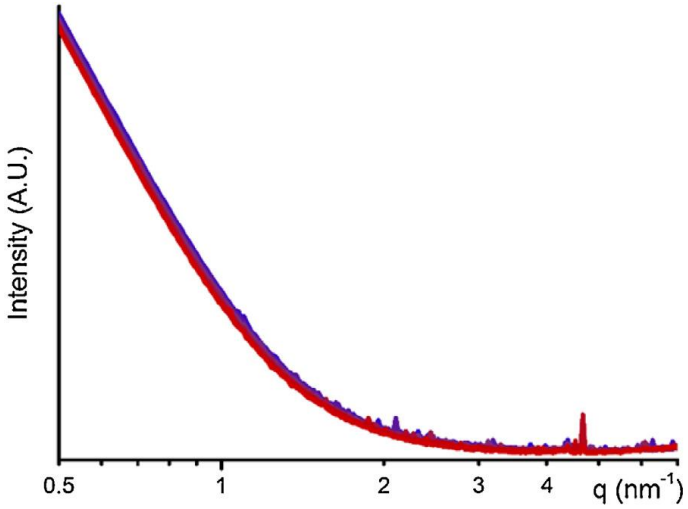

Fig. 3. Selection of SAXS patterns (in log–log scale) collected during activation of the bare P4VP support (i.e. without Pd) in H_2 from room temperature (bold red) to 200 °C (bold blue) with a heating rate of 2 °C min^{-1}. Same experimental set-up as in Fig. 1b. (For interpretation of the references to colour in this figure legend, the reader is referred to the web version of this article).

3.1.2. DRIFT spectroscopy

Successively, DRIFT spectroscopy was employed to monitor in situ reduction of P4VP/$Pd(OAc)_2$ in presence of gaseous H_2 as a function of temperature. Fig. 4 shows the DRIFT spectrum of bare P4VP support (black) and of

the P4VP/$Pd(OAc)_2$ catalyst (red). The spectrum of P4VP is dominated by the absorption bands due to the vibrational modes of the benzyl and pyridyl rings.

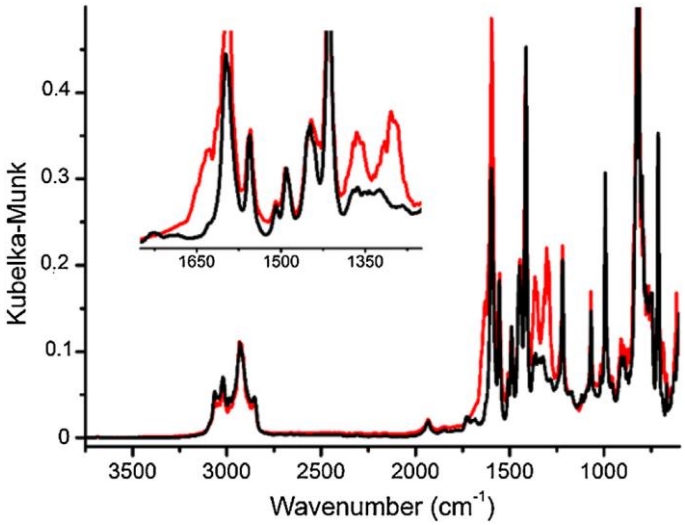

Fig. 4. DRIFT spectra of bare P4VP before (black) and after $Pd(OAc)_2$ impregnation (red). The inset shows a magnification of the spectral region where the main absorption bands of the polymer and of palladium (II) acetate contribute. (For interpretation of the references to colour in this figure legend, the reader is referred to the web version of this article).

The absorption bands characteristic of the pyridyl group shift after insertion of $Pd(OAc)_2$. In particular, the two bands at ν = 1596 and 1414 cm^{-1}, corresponding to the 8a and 19b vibrational modes of pyridyl functional group, shift to ν = 1640 and 1430 cm^{-1} [53]. Similar shifts of the IR absorption bands typical of the pyridyl groups in P4VP were reported in literature for several P4VP/metal complexes [54–57], and interpreted in terms of a strong interaction between the pyridyl groups of the polymer and the coordinated metal precursors. Hence, DRIFT spectra demonstrate that insertion of palladium (II) acetate into the P4VP scaffold occurs via chemical interactions involving the pyridyl groups in the polymer. In addition, the spectrum of P4VP/$Pd(OAc)_2$ shows two intense absorption bands at 1365 and 1315 cm^{-1}, which are typical of acetate ligands in a monodentate coordination [23]. Fig. 5a shows the DRIFT spectra of P4VP/$Pd(OAc)_2$ collected during reduction in H_2 at increasing temperature from 25 (blue curve) to 200 °C (red curve). Treatment in H_2 causes the decomposition of the palladium (II) acetate precursor, as demonstrated by the gradual disappearance of the absorption bands at 1365 and 1315 cm^{-1}, related to the acetate groups. Acetic acid is detected as intermediate (absorption bands close to 1725 cm^{-1}), but it is not stable at high reduction temperature. The inset in Fig. 5a shows the intensity of the absorption band at 1365 cm^{-1} (taken here as a reference for the acetate ligands) as a function of temperature. It is evident that reduction begins at a temperature around 110 °C, in good agreement with the XANES-SAXS results discussed above. In order to characterize the palladium nanoparticles obtained at the end of the reduction process, we dosed CO at room temperature at the end of the reduction step (hereafter P4VP/Pd sample). Indeed, DRIFT spectroscopy of CO adsorbed at room temperature is a well-established technique to quantitatively and qualitatively characterize the surface properties of palladium nanoparticles [21,31,58–61]. Fig. 5b shows the DRIFT spectrum of CO adsorbed on P4VP/Pd sample collected after having saturated the environmental chamber, upon decreasing and the sequence of spectra collected upon decreasing the CO concentration in the flow. At the maximum CO coverage (θ_{max}), two absorption bands are observed at 2040 and 1890 cm^{-1}, overlapped to the intense bands due to gaseous CO at 2143 cm^{-1} [62]. The first two bands are easily assigned to linear carbonyl and bridged carbonyl species respectively [21,31,58–61]. Both bands are quite broad, suggesting the presence of a great variety of carbonyls, as expected for highly defective and/or amorphous nanoparticles [58,63,64]. Hence, the data shown in Fig. 5 demonstrate that DRIFT spectroscopy allows to follow the reduction of P4VP/$Pd(OAc)_2$ as a function of

temperature and simultaneously to obtain information on the formed palladium nanoparticles. For this reason, in the following we apply the same technique to obtain preliminary information on the effect of alcohols on the same sample.

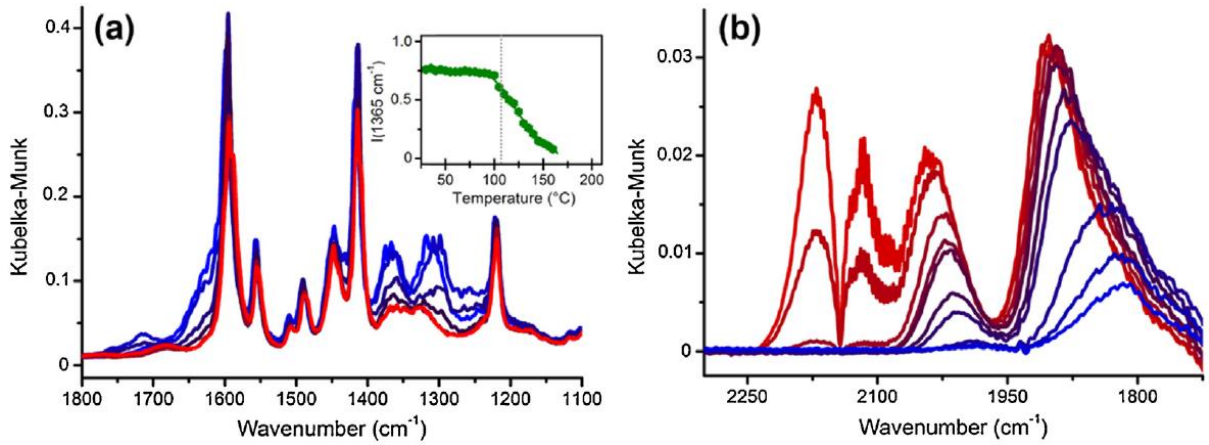

Fig. 5. Part (a) DRIFT spectra of P4VP/Pd(OAc)$_2$ during the thermal treatment in presence of H_2. The temperature rises going from blue (25 °C) to red (200 °C) spectra. The inset shows the evolution as a function of temperature of the intensity of the IR absorption band at 1365 cm^{-1}, which is characteristic of the acetate ligands. Part (b) DRIFT spectra (in the ν(CO) region) of CO adsorbed at room temperature on the P4VP/Pd sample obtained from P4VP/Pd(OAc)$_2$ after reduction in H_2, as a function of the CO concentration (from red at θ_{max}, to blue at θ_{min}). The spectra were subtracted from the spectrum of the sample prior to CO adsorption. (For interpretation of the references to colour in this figure legend, the reader is referred to the web version of this article).

3.2. Thermal behavior of P4VP/Pd(OAc)$_2$ in presence of alcohols: innocent or active?

The thermal behavior of P4VP/Pd(OAc)$_2$ was tested in the presence of different alcohols (ethanol and 2-propanol). As discussed in the introduction, alcohols are often used as solvents in reactions catalyzed by Pd-based catalysts [33], or they may be used even as reactants [34–41]. Therefore, it is important to clarify if they are innocent toward the catalyst, or if they may react with it and eventually lead to its final deactivation.

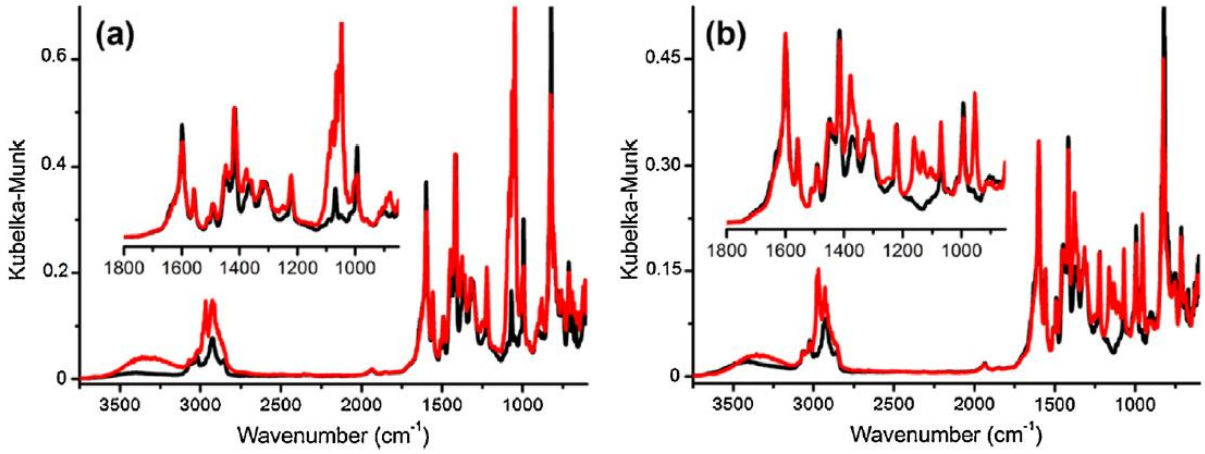

Fig. 6. DRIFT spectra of P4VP/Pd(OAc)$_2$ before (black) and after (red) interaction with ethanol (part a) and 2-propanol (part b). Insets show a magnification of the area of interest for the control of the reduction process. (For interpretation of the references to colour in this figure legend, the reader is referred to the web version of this article).

Fig. 6a shows the DRIFT spectra of P4VP/Pd(OAc)$_2$ before and after dosing the vapour pressure of ethanol; Fig. 6b shows the same for 2-propanol. In both cases, the DRIFT spectra collected at room temperature in presence of the alcohols are dominated by the intense absorption bands due to the alcohols physisorbed in the polymer (ν(OH) in the 3500–3100 cm^{-1} region, ν(CH) in the 3000–2800 cm^{-1} region, δ(CH) around

1400 cm^{-1}, and ν(C-O) close to 1000 cm^{-1}). In particular, the most intense bands are observed at 1050 cm^{-1} for ethanol and at 955 cm^{-1} for 2-propanol, and correspond to the ν(C-O) vibrational modes of condensed alcohols.

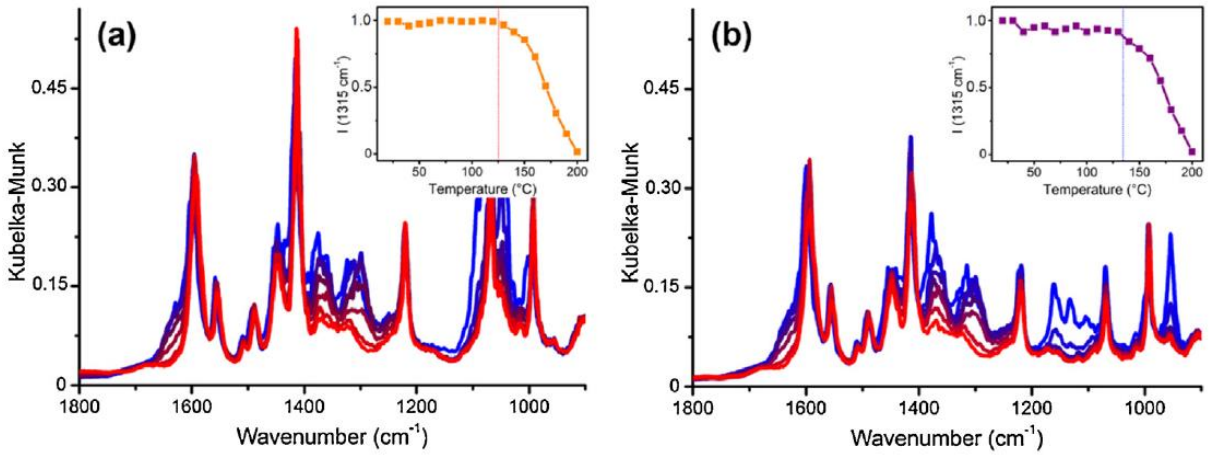

Fig. 7. Evolution of the DRIFT spectra during the thermal treatment of P4VP/$Pd(OAc)_2$ in presence of ethanol (part a) and 2-propanol (part b). Colour change from blue to red with the rise of the temperature; temperature ramp of 2 °C·min^{-1}, T_{final} = 200 °C. The inset shows the evolution as a function of temperature of the intensity of the IR absorption band at 1315 cm^{-1}, which is characteristic of the acetate ligands. (For interpretation of the references to colour in this figure legend, the reader is referred to the web version of this article).

Fig. 7 shows the sequence of DRIFT spectra collected during the thermal treatment of P4VP/$Pd(OAc)_2$ in presence of the two alcohols from 25 (blue curve) to 200 °C (red curve). Upon increasing temperature up to around 130 °C (i.e. above the boiling temperature of the two alcohols), the IR absorption bands due to physisorbed alcohols gradually disappear. At higher temperature, the absorption bands at 1365 and 1315 cm^{-1} due to acetate ligands begin to decrease in intensity, indicating that palladium (II) acetate is gradually decomposed. Insets in Fig. 7 show the trend of palladium (II) acetate decomposition as a function of temperature. However, the disappearance of the bands due to species is not sufficient to prove the formation of the metal nanoparticles; therefore also in these cases the use of CO as probe molecule was exploited to check the effective formation of palladium nanoparticles and to characterize them.

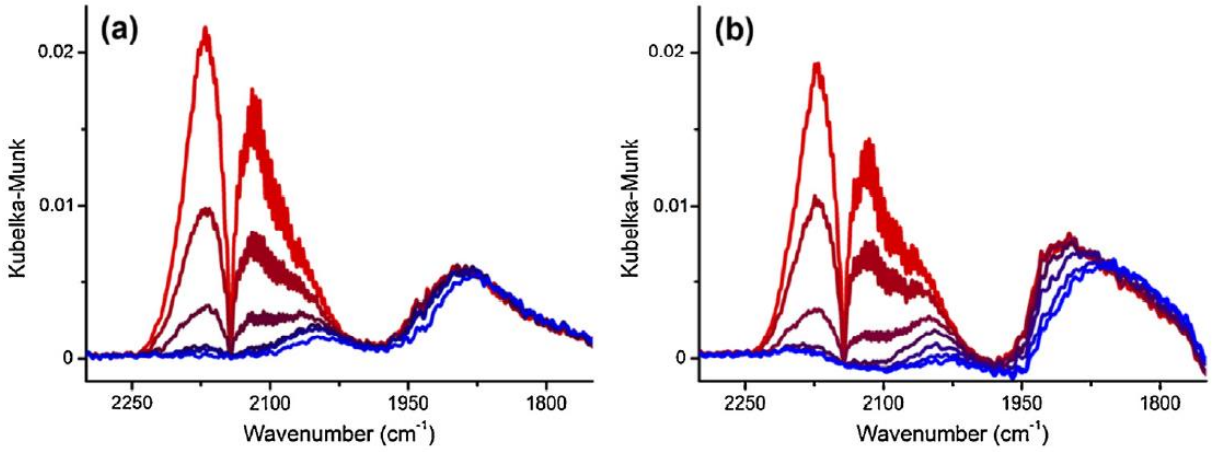

Fig. 8. DRIFT spectra (in the ν(CO) region) of CO adsorbed at room temperature on the P4VP/Pd sample obtained from P4VP/$Pd(OAc)_2$ after thermal treatment in ethanol (part a) and 2-propanol (part b), as a function of CO concentration (from red at θ_{max}, to blue at θ_{min}). The spectra were subtracted from the spectrum of the sample prior to CO adsorption. (For interpretation of the references to colour in this figure legend, the reader is referred to the web version of this article).

Fig. 8 shows the sequence of DRIFT spectra of CO adsorbed at room temperature on the P4VP/Pd samples after the thermal treatment in alcohols, as a function of CO concentration. In both cases, two weak absorption bands are observed, overlapped to the roto-vibrational profile of gaseous CO, with maxima at 2040 and 1890 cm^{-1} at θ_{max}, which are assigned to linear and bridged carbonyl species on defective/amorphous palladium nanoparticles respectively. Hence, these spectra demonstrate that alcohols are not innocent and have the ability to reduce palladium (II) acetate, although their reduction potential is not as high as for H_2. Further measurements with additional characterization techniques (including simultaneous XANES-SAXS and TEM measurements) are planned in the near future to get more insights in the formation of palladium nanoparticles in presence of alcohols.

4. Conclusions

The use of simultaneous XANES-SAXS techniques, combined with DRIFT spectroscopy, allowed us to monitor the reactivity of $Pd(OAc)_2$ in a P4VP polymer towards H_2 as a function of temperature. It was found that the pyridyl functional groups in the polymer plays a fundamental role at two different levels: (1) in the stabilization of the palladium (II) acetate precursor, which occurs through a direct interaction of the pyridyl groups with the Pd^{2+} cations, and the consequent adjustment of the acetate ligands in a monodentate configuration [23]; (2) in the stabilization of the palladium nanoparticles obtained upon reduction in H_2 at increasing temperature. As a consequence of point (1), the reduction of palladium (II) acetate in P4VP occurs at a higher temperature compared to reduction of palladium (II) acetate dispersed in a similar polymer without functional groups [22]. As a consequence of point (2), the formed palladium nanoparticles are smaller, due to the stabilization via direct covalent interaction with the nitrogen-containing ligands [21]. The data discussed in the first part of the manuscript demonstrate that DRIFT spectroscopy in operando allows to follow the reduction of P4VP/$Pd(OAc)_2$ as a function of temperature and simultaneously to obtain information on the formed palladium nanoparticles. In the second part of the manuscript we applied infrared spectroscopy to obtain preliminary information on the effect of alcohols on P4VP/$Pd(OAc)_2$. We demonstrated that alcohols (ethanol and 2-propanol) in the gas phase act as reducing agents for $Pd(OAc)_2$.The reaction was successfully followed by means of DRIFT spectroscopy, by monitoring the disappearance of the IR bands due to $Pd(OAc)_2$. The obtained palladium nanoparticles were preliminarily characterized by means of CO used as probe molecule. These data demonstrate that alcohols have the potential to reduce palladium salts to palladium nanoparticles, already in the gas phase.

Acknowledgements

Carlo Lamberti acknowledges the Mega-grant of the Russian Federation Government to support scientific research at the Southern Federal University (Rostov-on-Don), No. 14.Y26.31.0001.

References

[1] N. Pernicone, M. Cerboni, G. Prelazzi, F. Pinna, G. Fagherazzi, Catal. Today 44 (1998) 129.

[2] H.-U. Blaser, A. Indolese, A. Schnyder, H. Steiner, M. Studer, J. Mol. Catal. A: Chem. 173 (2001) 3.

[3] E. Groppo, G. Agostini, A. Piovano, N.B. Muddada, G. Leofanti, R. Pellegrini, G.Portale, A. Longo, C. Lamberti, J. Catal. 287 (2012) 44.

[4] S. Klingelhöfer, W. Heitz, A. Greiner, S. Oestreich, S. Förster, M. Antonietti, J. Am. Chem. Soc. 119 (1997) 10116.

[5] L.M. Bronstein, D.M. Chernyshov, I.O. Volkov, M.G. Ezernitskaya, P.M.Valetsky, V.G. Matveeva, E.M. Sulman, J. Catal. 196 (2000) 302.

[6] R. Akiyama, S. Kobayashi, Angew. Chem. Int. Ed. 40 (2001) 3469.

[7] R. Akiyama, S. Kobayashi, J. Am. Chem. Soc. 125 (2003) 3412.

[8] U. Schlotterbeck, C. Aymonier, R. Thomann, H. Hofmeister, M. Tromp, W.Richtering, S. Mecking, Adv. Funct. Mater. 14 (2004) 999.

[9] R. Shenhar, T.B. Norsten, V.M. Rotello, Adv. Mater 17 (2005) 657.

[10] H. Song, R.M. Rioux, J.D. Hoefelmeyer, R. Komor, K. Niesz, M. Grass, P. Yang,G.A. Somorjai, J. Am. Chem. Soc. 128 (2006) 3027.

[11] C. Moreno-Marrodan, P. Barbaro, M. Catalano, A. Taurino, Dalton Trans. 41 (2012) 12666.

[12] R. Herbois, S. Noel, B. Leger, L. Bai, A. Roucoux, E. Monflier, A. Ponchel, Chem. Commun. 48 (2012) 3451.

[13] F. Novio, D. Monahan, Y. Coppel, G. Antorrena, P. Lecante, K. Philippot, B.Chaudret, Chem. - Eur. J. 20 (2014) 1287.

[14] N.T.S. Phan, M. Van Der Sluys, C.W. Jones, Adv. Synth. Catal. 348 (2006) 609.

[15] H. Bönnemann, Ryan M. Richards, Eur. J. Inorg. Chem. 2001 (2001) 2455.

[16] B. Corain, K. Jerabek, P. Centomo, P. Canton, Angew. Chem. Int. Ed. 43 (2004) 959.

[17] L.S. Ott, R.G. Finke, Coord. Chem. Rev. 251 (2007) 1075.

[18] B.M.L. Dioos, I.F.J. Vankelecom, P.A. Jacobs, Adv. Synth. Catal. 348 (2006) 1413.

[19] S. Kobayashi, R. Akiyama, Chem. Commun. 2003 (2003) 449.

[20] C. Pan, K. Pelzer, K. Philippot, B. Chaudret, F. Dassenoy, P. Lecante, M.-J.Casanove, J. Am. Chem. Soc. 123 (2001) 7584.

[21] E. Groppo, W. Liu, O. Zavorotynska, G. Agostini, G. Spoto, S. Bordiga, C.Lamberti, A. Zecchina, Chem. Mater. 22 (2010) 2297.

[22] E. Groppo, G. Agostini, E. Borfecchia, L. Wei, F. Giannici, G. Portale, A. Longo, C.Lamberti, J. Phys. Chem. C 118 (2014) 8406.

[23] E. Groppo, G. Agostini, E. Borfecchia, A. Lazzarini, W. Liu, C. Lamberti, F.Giannici, G. Portale, A. Longo, ChemCatChem 7 (2015) 2188.

[24] D. Grosso, F. Ribot, C. Boissiere, C. Sanchez, Chem. Soc. Rev. 40 (2011) 829.

[25] B. Ingham, Crystallogr. Rev. 21 (2015) 229.

[26] L. Suber, G. Campi, Nanotechnol. Rev. 1 (2012) 57.

[27] S. Bordiga, E. Groppo, G. Agostini, J.A. van Bokhoven, C. Lamberti, Chem. Rev.113 (2013) 1736.

[28] C. Garino, E. Borfecchia, R. Gobetto, J.A. van Bokhoven, C. Lamberti, Coord.Chem. Rev. 277–278 (2014) 130.

[29] L. Mino, G. Agostini, E. Borfecchia, D. Gianolio, A. Piovano, E. Gallo, C.Lamberti, J. Phys. D: Appl. Phys. 46 (2013) 72.

[30] M.B. Mitchell, Fundamentals and applications of diffuse reflectance infrared fourier transform (DRIFT) spectroscopy, in: M.W. Urban, C.D. Crave (Eds.),Structure-Property Relations in Polymers, American Chemical Society, 1993,p. 351.

[31] C. Lamberti, A. Zecchina, E. Groppo, S. Bordiga, Chem. Soc. Rev. 39 (2010) 4951.

[32] S. Bordiga, C. Lamberti, F. Bonino, A. Travert, F. Thibault-Starzyk, Chem. Soc. Rev. 44 (2015) 7262.

[33] O. Navarro, R.A. Kelly, S.P. Nolan, J. Am. Chem. Soc. 125 (2003) 16194.

[34] G. Giachi, M. Frediani, W. Oberhauser, E. Passaglia, J. Polym. Sci. A: Pol. Chem.50 (2012) 2725.

[35] C.M. Park, M.S. Kwon, J. Park, Synthesis 2006 (2006) 3790.

[36] S. Rautiainen, O. Simakova, H. Guo, A.-R. Leino, K. Kordás, D. Murzin, M.Leskelä, T. Repo, Appl. Catal. A: Gen 485 (2014) 202.

[37] E. Sadeghmoghaddam, H. Gu, Y.-S. Shon, ACS Catal. 2 (2012) 1838.

[38] S.S. Stahl, Angew. Chem. Int. Ed. 43 (2004) 3400.

[39] B.A. Steinhoff, I.A. Guzei, S.S. Stahl, J. Am. Chem. Soc. 126 (2004) 11268.

[40] B.A. Steinhoff, S.S. Stahl, Org. Lett. 4 (2002) 4179.

[41] O.M. Wilson, M.R. Knecht, J.C. Garcia-Martinez, R.M. Crooks, J. Am. Chem. Soc.128 (2006) 4510.

[42] A. Longo, G. Portale, W. Bras, F. Giannici, A.M. Ruggirello, V. Turco Liveri, Langmuir 23 (2007) 11482.

[43] S. Nikitenko, A.M. Beale, A.M.J. van der Eerden, S.D.M. Jacques, O. Leynaud, M.G. O'Brien, D. Detollenaere, R. Kaptein, B.M. Weckhuysen, W. Bras, J.Synchrotron Radiat. 15 (2008) 632.

[44] B. Ravel, M. Newville, J. Synchrotron Radiat 12 (2005) 537.

[45] G. Portale, A. Longo, Small-angle X-ray scattering for the study of nanostructures and nanostructured materials, in: C. Lamberti, G. Agostini (Eds.), Characterization of Semiconductor Heterostructures and Nanostructures, 2nd edition, Elsevier, Amsterdam, 2013, p. 175.

[46] B. Abécassis, F. Testard, O. Spalla, P. Barboux, Nano Lett. 7 (2007) 1723.

[47] B. Abécassis, F. Testard, Q. Kong, B. Francois, O. Spalla, Langmuir 26 (2010) 13847.

[48] M. Harada, N. Tamura, M. Takenaka, J. Phys. Chem. C 115 (2011) 14081.

[49] G. Agostini, C. Lamberti, R. Pellegrini, G. Leofanti, F. Giannici, A. Longo, E.Groppo, ACS Catal. 4 (2014) 187.

[50] G. Agostini, R. Pellegrini, G. Leofanti, L. Bertinetti, S. Bertarione, E. Groppo, A.Zecchina, C. Lamberti, J. Phys. Chem. C 113 (2009) 10485.

[51] G. Agostini, E. Groppo, A. Piovano, R. Pellegrini, G. Leofanti, C. Lamberti, Langmuir 26 (2010) 11204.

[52] G. Agostini, A. Piovano, L. Bertinetti, R. Pellegrini, G. Leofanti, E. Groppo, C.Lamberti, J. Phys. Chem. C 118 (2014) 4085.

[53] E. Groppo, M.J. Uddin, O. Zavorotynska, A. Damin, J.G. Vitillo, G. Spoto, A.Zecchina, J. Phys. Chem. C 112 (2008) 19493.

[54] E. Groppo, M.J. Uddin, S. Bordiga, A. Zecchina, C. Lamberti, Angew. Chem. Int. Ed. 120 (2008) 9409.

[55] M.P. McCurdie, L.A. Belfiore, Polymer 40 (1999) 2889.

[56] A.J. Pardey, A.D. Rojas, J.E. Yánez, P. Betancourt, C. Scott, C. CarlosChinea, D.Urbina, C. Moronta, Longo Polyhedron 24 (2005) 511.

[57] K.H. Wu, Y.R. Wang, W.H. Hwu, Polym. Degrad. Stab. 79 (2003) 195.

[58] S. Bertarione, C. Prestipino, E. Groppo, D. Scarano, G. Spoto, A. Zecchina, R.Pellegrini, G. Leofanti, C. Lamberti, Phys. Chem. Chem. Phys. 8 (2006) 3676.

[59] E. Groppo, S. Bertarione, F. Rotunno, G. Agostini, D. Scarano, R. Pellegrini, G.Leofanti, A. Zecchina, C. Lamberti, J. Phys. Chem. C 111 (2007) 7021.

[60] F.M. Hoffmann, Surf. Sci. Rep 3 (1983) 107.

[61] E. Ozensoy, D. Wayne Goodman, Phys. Chem. Chem. Phys. 6 (2004) 3765.

[62] C. Lamberti, C. Morterra, S. Bordiga, G. Cerrato, D. Scarano, Vib. Spectrosc. 4 (1993) 273.

[63] J.S. Bradley, E.W. Hill, S. Behal, C. Klein, A. Duteil, B. Chaudret, Chem. Mater. 4 (1992) 1234.

[64] J.S. Bradley, J.M. Millar, E.W. Hill, S. Behal, J. Catal. 129 (1991) 530.